RSC Advances

PAPER

View Article Online
View Journal | View Issue

Cite this: *RSC Adv.*, 2015, **5**, 85523

Detection of a high photoresponse at zero bias from a highly conducting ZnO:Ga based UV photodetector

Pankaj Sharma,[a] Rohit Singh,[a] Vishnu Awasthi,[a] Sushil K. Pandey,[b] Vivek Garg[a] and Shaibal Mukherjee*[a]

Received 15th July 2015
Accepted 5th October 2015

DOI: 10.1039/c5ra13921j

www.rsc.org/advances

Ga-doped ZnO (GZO) based ultraviolet photodetectors (PDs) were fabricated by dual ion beam sputtering with a metal–semiconductor–metal structure. The room-temperature operable PD demonstrated responsivity of 58 mA W^{-1} at zero bias, which is 15 times larger than that reported on similar material grown by a different physical vapour deposition process, with internal and external quantum efficiency values of ~22.5% and 37.4%. The unbiased photodetection is attributed to the tunnelling of electrons due to heavy doping of GZO and built-in electric field due to different barriers at the two metal semiconductor contacts. The asymmetry in the electrodes was investigated by temperature-dependent current–voltage measurements.

Introduction

In recent times, research on ZnO based ultraviolet (UV) photodetectors (PDs) has gained interest due to their unique properties, such as direct wide band gap of 3.37 eV, large exciton binding energy of 60 meV, high radiation hardness, and hence they find applications in air quality monitoring, flame detection and defence applications, such as UV communications and missile warning systems.[1,2] ZnO films for UV PDs have been deposited by various techniques such as magnetron sputtering,[3] molecular beam epitaxy,[4] and pulsed laser deposition.[5] Moreover various studies based on Ga-doped ZnO (GZO) thin films for UV PDs have been reported.[6–9] However, to the best of the authors' knowledge, there are no reports on the detailed study of GZO based UV PD fabricated by dual ion beam sputtering deposition (DIBSD).[10,11] Different PD structures such as photoconductive, Schottky, metal semiconductor metal (MSM), p–n and p–i–n junction based on ZnO material have been reported. However, MSM structure is preferred over others for UV PD applications because of its attractive advantages such as fabrication simplicity, single active layer requirement, and high gain.[12]

Since almost all kind of photodetectors requires external supply for their operation, it is highly desired to have PDs based on self-powered mechanism. These PDs are critical in terms of energy saving point of view and are preferred for long-term monitoring of air-pollution and wastewater. To the best of our knowledge the reports on unbiased photoresponse of ZnO based MSM photodetectors are still rare. Instead, recently Bai *et al.* and Ni *et al.* have reported similar results, for ZnO based heterostructures.[13,14] In this work, we discuss the phenomenon of zero bias photoresponse of GZO thin film PD, grown by DIBSD system, by investigating the electron transport mechanism through Au/GZO interface. In our GZO based photodetector, the internal quantum efficiency (IQE) at zero bias was as high as 37% with ultraviolet to visible rejection ratio of more than five orders.

Experimental

GZO film, with a thickness of 350 nm, employed as active layer of photodetector was grown on Si (100) by DIBSD using 3 at% GZO ceramic target. Other relevant growth details are mentioned elsewhere.[15] The deposition was carried out in Ar ambient (5 sccm) at varying substrate temperatures from 200 to 600 °C (samples S2 to S6). Finally, the UV PDs (D2 to D6) were fabricated by depositing 50 nm thick Au interdigitated contacts on GZO films by magnetron sputtering at room temperature. The mobility and carrier concentrations were measured by four-probe Hall measurement technique in van der Pauw geometry. X-Ray diffraction (XRD) of films was carried out using a Rigaku X-ray diffractometer with Cu K alpha radiation ($\lambda = 1.54$ Å). Current–voltage (I–V) measurements were performed using Keithley 2612 sourcemeter and Everbeing cryogenic probe station. Thickness and the optical constants of the films were determined by J. A. Woollam spectroscopic ellipsometer. Hiden secondary ion mass spectroscopy (SIMS) workstation with oxygen ion gun of energy up to 5 keV was used to verify the

[a]*Hybrid Nanodevice Research Group (HNRG), Indian Institute of Technology, Indore 453446, India. E-mail: shaibal@iiti.ac.in; Fax: +91-731-2361482; Tel: +91-732-4240704*

[b]*Department of Electrical Engineering, Indian Institute of Technology Bombay, Mumbai 400076, India*

presence of Ga in GZO film. The spectral responses and the quantum efficiency of the fabricated devices were characterized with Bentham photovoltaic characterization system consisting of 150 W Xe lamp, chopper, monochromator, and lock-in amplifier.

Results and discussion

XRD of GZO films deposited at various growth temperatures (T_g) are shown in Fig. 1(a). It can clearly be observed that all GZO films have a preferred *c*-axis orientation perpendicular to the substrate. No metallic Zn or Ga or any of Ga oxide characteristic peaks were observed in XRD pattern suggesting that Ga atoms have substituted Zn atoms effectively without changing the original hexagonal structure of ZnO.[16] The position of (002) peak and its corresponding full-width at half-maximum (FWHM) and grain size, as estimated by Scherrer's formula[17] are populated in Table 1. Moreover, the values of external and internal quantum efficiencies (EQE and IQE) of all UV PDs are mentioned in Table 1. The angular position of (002) peaks is much close to that of ZnO powder peak (34.34°) indicating stress free film deposition. As represented in Fig. 1(a), as T_g was increased from 200 to 300 °C, intensity of (002) peak increased on account of increase in the dopant atomic energy that allowed the dopants to move from interstitial and/or grain boundary regions into the Zn lattice sites, resulting in an increase in the crystallinity along with higher carrier concentration.[16] However, the (002) peak intensity declined with further increase in T_g beyond 300 °C, indicating a reduced crystalline quality with higher T_g (400–600 °C).[18] The FWHM of (002) diffraction peak is the smallest at $T_g = 300$ °C, indicating the largest grain size and highest crystalline quality. Moreover, the grain size increases with the increase in T_g from 200 to 300 °C, whereas it reduces with further increase in T_g.

The Hall measurement exhibited n-type conduction for all GZO films. This n-type conduction is due to Ga incorporation into GZO where Ga will occupy Zn sites and be ionized into Ga^{3+}. This process supplies one free electron to the conduction band for each Ga atom added. Fig. 1(b) shows the carrier concentration, mobility, and resistivity of GZO films as a function of T_g. The electrical resistivity of GZO film decreased marginally when T_g reached 300 °C and afterwards the resistivity increased sharply with higher T_g. A minimum resistivity value of 5.3×10^{-4} Ω cm is obtained at 300 °C. Similarly, the carrier concentration demonstrated an enhancement[19] up to 300 °C and then reduced gradually with further increase in T_g. The trend of variation of electrical resistivity and carrier concentration was guided by the crystallinity of GZO films, as depicted in Fig. 1(a).[19] However, carrier mobility exhibited an initial increase with increasing T_g from 200 to 400 °C and then decreased sharply at 500 °C. This decay in mobility, with carrier concentration of $\sim 10^{20}$ cm^{-3}, may have been caused by ionized

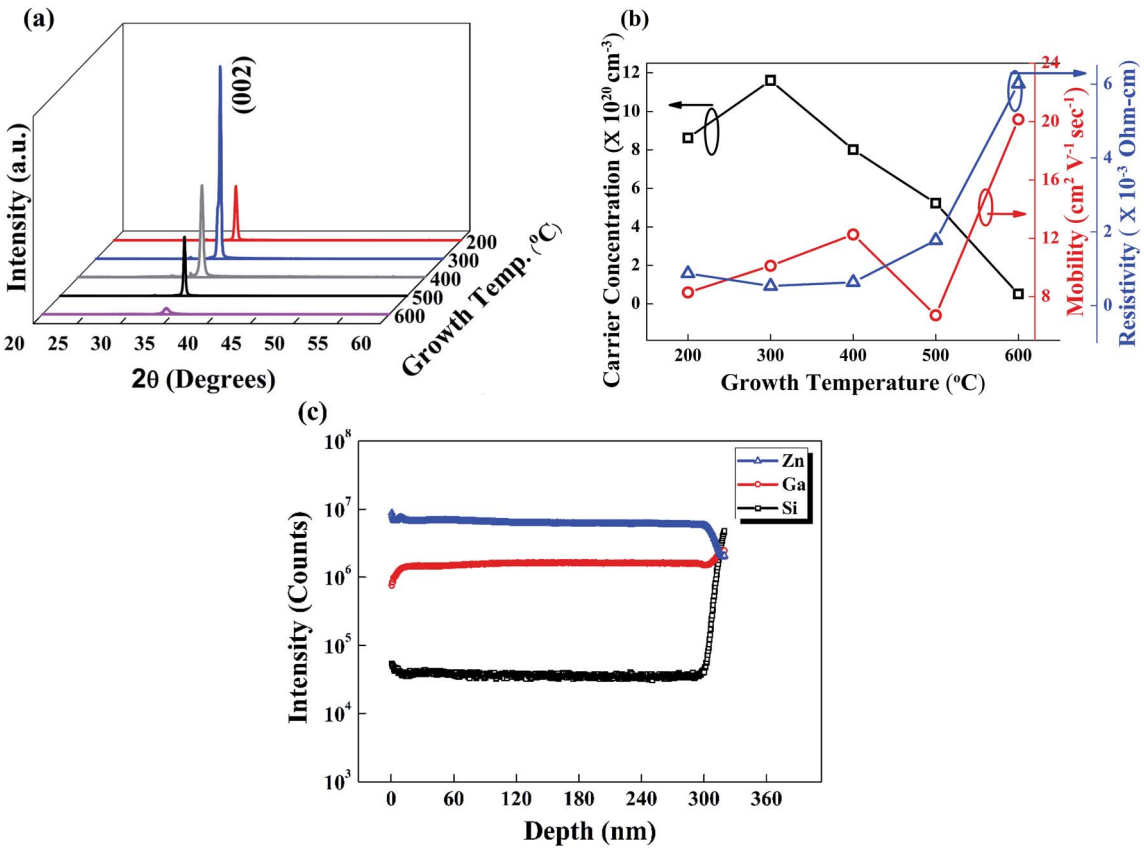

Fig. 1 (a) XRD patterns of GZO films grown at different T_g, (b) carrier concentration, mobility, and resistivity of GZO films, (c) SIMS depth profile of as-grown GZO film.

Table 1 Peak position, FWHM, grain size of GZO films and EQE, and IQE of GZO based UV PDs

Sample (device)	Growth temperature (°C)	Peak position 2θ (degree)	FWHM (degree)	Grain size (nm)	EQE (%)	IQE (%)
S2 (D2)	200	34.05	0.32	27.1	6.11	10.18
S3 (D3)	300	34.3	0.2	43.4	22.5	37.41
S4 (D4)	400	34.25	0.36	24.1	3.21	5.35
S5 (D5)	500	34.32	0.3	28.9	1.01	1.68
S6 (D6)	600	34.27	0.68	12.7	0.99	1.65

impurity scattering.[20] As it is well known that mobility in heavily doped ZnO is controlled by various factors such as dislocations, grain boundary scattering, ionized impurity scattering, and carrier concentration *etc.*,[20] a sharp increase in mobility at 600 °C may be correlated to lesser scattering effect with comparatively low electron concentration at 600 °C.[21] The depth profile of the main elements in an as-grown GZO film (S3) is shown in Fig. 1(c). It is evident that Ga has been clearly detected, and its concentration profile is quite flat throughout the film depth.

Shadow masking technique was deployed to fabricate MSM-type device structure using a metal interdigitated mask. The electrode fingers were 5 mm long, 100 μm wide, and the spacing between two adjacent fingers were 200 μm. The schematic diagram of the fabricated device is shown in Fig. 2(a). Fig. 2(b) shows the absorption spectra of sample S3 that clearly depicts that the layer has a strong absorption to photons with wavelength shorter than 370 nm, while it is almost transparent to those with wavelength longer than 400 nm. The spectral response measurements of PD, as shown in Fig. 2(c), were carried out from 300 to 500 nm. The photo-responsivity was measured in unbiased (zero bias) mode as well as applying a small positive bias voltage, 1 V at room temperature. It is observed that the device D3 has the highest responsivity of 58 mA W^{-1} at zero bias, which is ~15 times and 3 times larger than that reported in ref. 8 and 22, respectively. The response peak is centered on 325 nm and a cut-off wavelength around 370 nm corresponding to the band gap energy of GZO films. Table 2 compares the various reports on zero bias photo response from available literature.[8,22,23] Responsivity (R_i) of the photodetector can be expressed as $R_i = \eta g(q\lambda/hc)$,[9] where λ is wavelength, q is electronic charge, h is the Plank's constant, c is light velocity in free-space, η is EQE, and g is the gain. An increase in the quantum efficiency was observed on application of external bias exhibiting the photoconductive gain. Table 3 shows the values of absorption edge wavelength, as calculated using the inset of Fig. 2(b), and peak photoresponse wavelength, as evaluated from Fig. 2(c), of all GZO samples and corresponding devices. It is clear that the trend of variation of photoresponse peak wavelength is governed by that of absorption peak wavelength. Fig. 2(d) shows the spectral response of device D3 at zero and 1 V bias, respectively. Device IQE was determined by normalizing the EQE as IQE = EQE/(1 − R),[24] where R is the measured reflectance of the GZO layer. While the EQE at zero bias was measured to be ~22.5%, it reached to 48% at 1 V bias with an average photocurrent of 23 mA. A significantly higher value of IQE at zero bias was calculated to be 37.4%. On further increase in applied bias, the photocurrent reaches saturation and the measurement was limited by instrument capability. Moreover, photosensitivity measurements of the GZO PDs were performed by turning the continuous UV illumination at 325 nm ON and OFF at an applied bias of 1 V. Fig. 2(e) shows the photocurrent rise and decay as a function of time at an applied bias of 1 V. The device was kept in dark for 12 hours to stabilize and then exposed to UV radiation for 25 s. The rise time is defined as the time needed to reach 90% from 10% of the maximum photocurrent while the fall time is the time needed to reach 10% from 90% of the maximum photocurrent.[6] From Fig. 2(e), the values of rise time of 806 ms and fall time of 54 s were obtained for the GZO UV photodetector. The photosensitivity (S) can be expressed as $S = (I_{light} - I_{dark})/I_{dark}$,[11] where I_{light} and I_{dark} are the light and dark current with and without UV illumination, respectively. The values of photosensitivity and on/off ratio (I_{light}/I_{dark}) for device D3 were calculated to be 0.076 and 1.076, respectively. In order to assess the feasibility of using the MSM PD for practical applications, the responsivity measurement at zero bias voltage is conducted, as demonstrated in Fig. 2(f), for different intervals: (a) first 7 days, (b) 14 days, (c) 30 days, and (d) 60 days after device fabrication. It should be noted that the device was kept in normal ambient condition without having any passivation layer on top of it during the photo stability measurement.

In order to get a better understanding of the carrier transport phenomenon at the Au/GZO interface, one must recognize which transport process plays a dominant role in our MSM PD. Various models have been proposed to explain the excess leakage current through Au/GZO Schottky barrier but in general, the total current constitutes of both thermionic emission and tunnelling component. Assuming that thermionic emission is predominant, the reverse saturation current of a diode with tunnelling is given as,[25]

$$I = I_s\, e^{(V_r/E')} \quad (1)$$

where I_s is saturation current, V_r is applied reverse bias, and E' is the characteristic energy related to tunneling probability with E_{00} as the tunneling parameter given as

$$E_{00} = (q\hbar/2)(N_D/m^*\varepsilon_s)^{1/2} \quad (2)$$

where $\hbar$ is reduced Plank's constant, N_D is donor density, m^* is effective mass of electron, ε_s is relative dielectric constant of semiconductor. If $kT \gg qE_{00}$, thermionic emission prevails

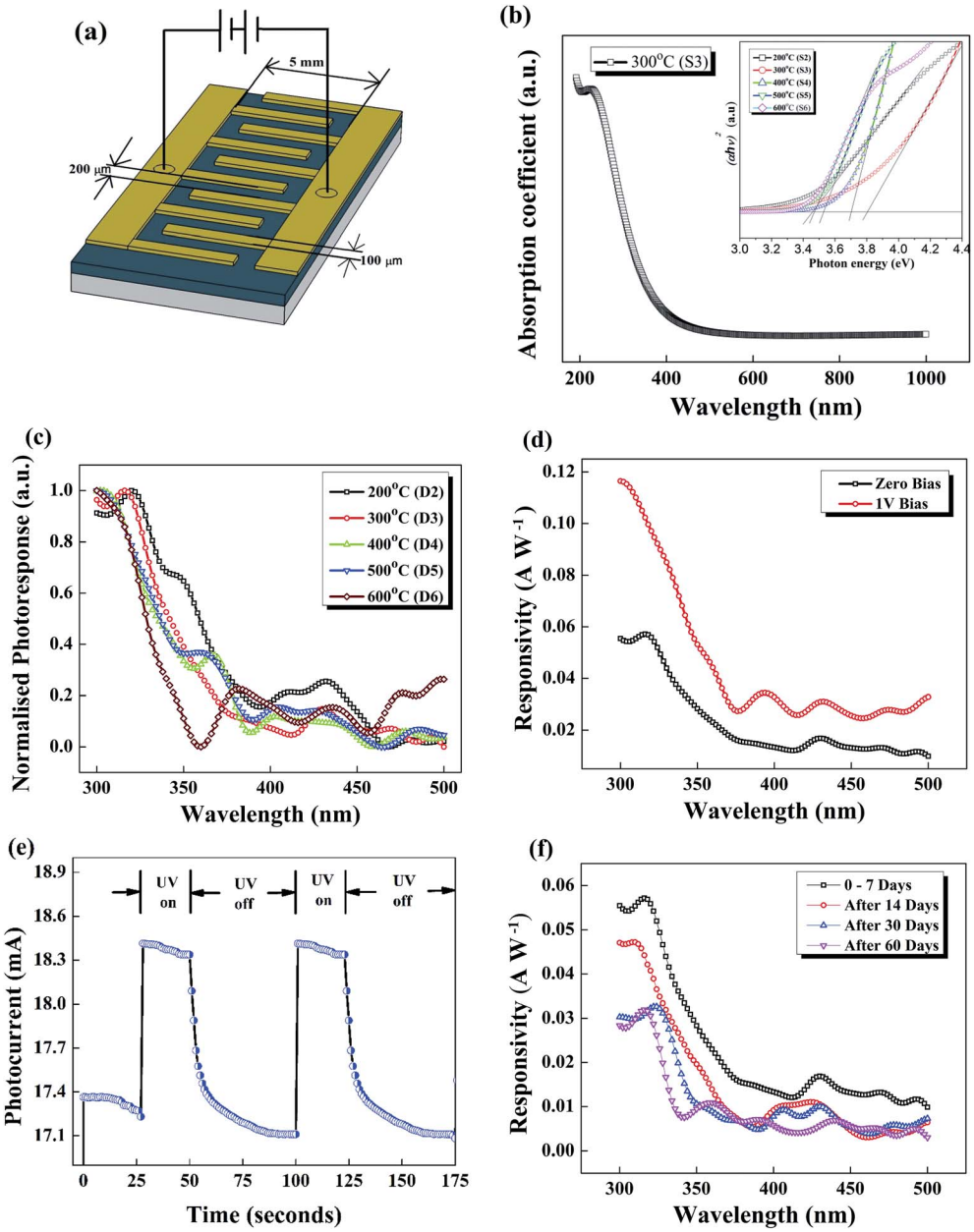

Fig. 2 (a) Schematic structure of MSM photodetector. (b) Optical absorption spectra of GZO film grown at $T_g = 300$ °C. Inset shows plot of $(\alpha h\nu)^2$ *vs.* $h\nu$ of all GZO films. (c) Normalized photoresponse of all fabricated devices. (d) Spectral responsivity of device D3 at zero bias and 1 V bias. (e) Time dependent photoresponse of GZO photodetector at 1 V bias. (f) Photo stability of UV PD at zero bias voltage for different time.

over tunnelling otherwise tunneling plays the dominant part when $kT < qE_{00}$. In our case, we have obtained a reasonable fit with the measured values as $m^* = 0.39m_0$, $\varepsilon_s = 8.12$ (ref. 26) and N_D of the order of 10^{20} from Hall results. By fitting the above parameters in eqn (2), the minimum value of E_{00} was calculated to be 74 meV for D5 and maximum value was found to be

Table 2 Comparative analysis of zero bias photoresponse from MSM-based UV PD in literature

Structure	Deposition technique	Peak responsivity	Ref.
MSM (Au–IGZO–Au)	Plasma assisted-PLD	4 mA W^{-1}	8
MSM (Au–ZnO–Au)	Plasma assisted-MBE	20 mA W^{-1}	22
MSM (Al–ZnO NW–Pt)	RF magnetron sputtering	1.82 mA W^{-1}	23
MSM (Au–GZO–Au)	Dual ion beam sputtering	58 mA W^{-1}	This work

Table 3 The absorption edge wavelength and peak of photoresponse wavelength

Sample (device)	Absorption edge (nm)	Peak photoresponse wavelength (nm)
S2 (D2)	356	355
S3 (D3)	325	325
S4 (D4)	340	365
S5 (D5)	351	355
S6 (D6)	363	375

374 meV for D3, which is almost 14 times higher than the thermal energy (25 meV), to conclude that tunnelling is the predominant mechanism responsible for the conduction in all the samples. The maximum value of E_{00} for D3 is justified from the fact that the grain size of S3 is the largest, as observed in Table 1, indicating a large surface area to volume ratio and hence increased mobility[20] and improved crystal quality resulting in enhanced photoresponsivity.[7]

In order to investigate the high photoresponse at zero applied bias, a model based on thin surface barrier[27] with asymmetric electrodes[28,29] is assumed. It is well known that surface barrier lowering occurs at metal–semiconductor interface[25,30] due to the presence to donor defect states, resulting in reduction of Schottky barrier width such that the electron can easily tunnel across the junction, as confirmed by above calculation. To establish the dissimilar characteristic of identically deposited Au electrodes on GZO films, *I*–*V* measurements for both forward and reverse bias voltages were performed in temperature ranging from 80 to 300 K. Indium contact was realized on top of GZO surface to form a perfect ohmic contact. Fig. 3(a) shows the temperature dependent ln(*I*)–*V* curves for Au1/GZO/In while Fig. 3(b) displays the temperature dependent ln(*I*)–*V* curves for Au2/GZO/In, where Au1 and Au2 are two Au contacts on GZO films, respectively. It is clearly observed that the current for Au1/GZO/In is temperature independent confirming the tunnelling of carriers, whereas current increases for Au2/GZO/In contacts demonstrating a relatively weaker Schottky behaviour. Moreover, Fig. 3(c) depicts *I*–*V* characteristics of both Au contacts at 80 and 300 K illustrating the clear inhomogeneity in the identically deposited electrodes.

The asymmetrical behaviour of Au electrodes may have been originated from dissimilar accumulation of surface/donor defect states at the interface of Au/GZO junction.[31] The variation in the generation of such interface defect states might have been resulted due to dissimilar surface damage triggered by sputtering of Au electrodes on GZO films. Based on the experimental results and analysis, the energy band diagram for GZO-based MSM PD in zero biased conditions is shown in Fig. 3(d).

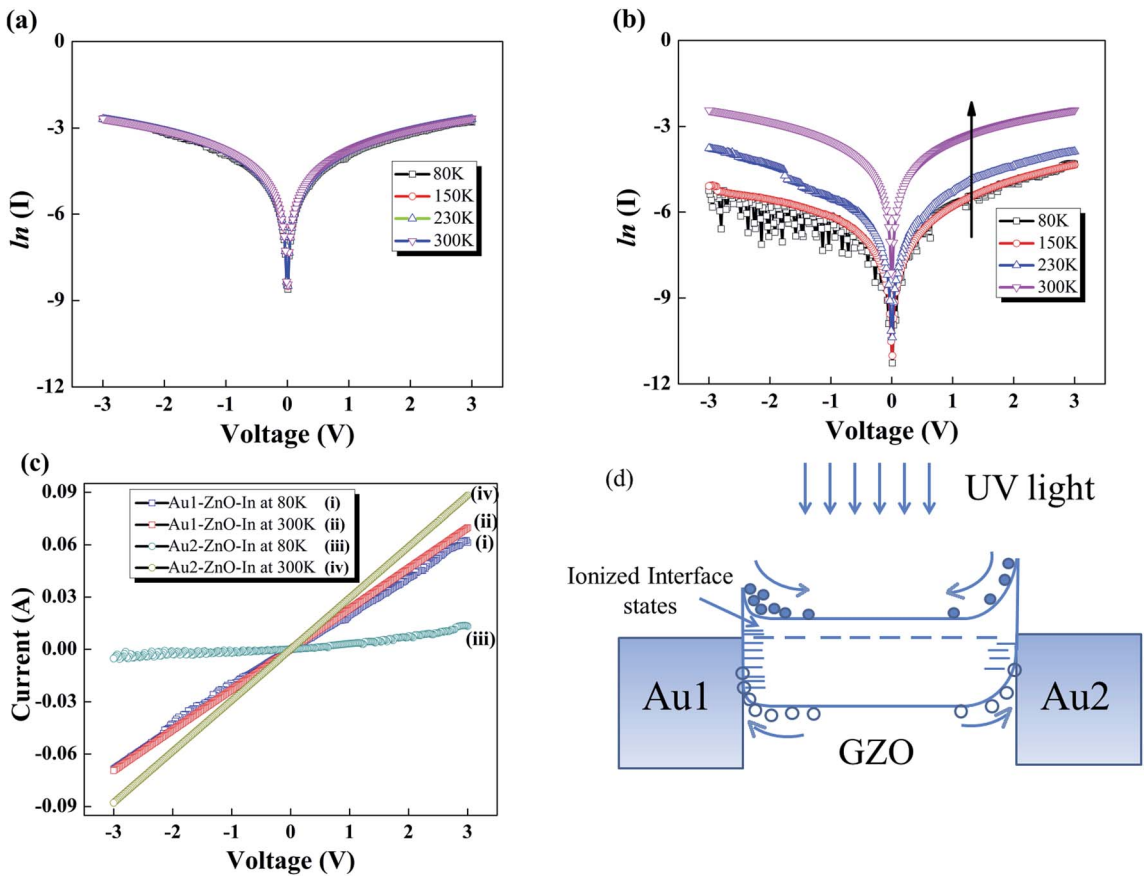

Fig. 3 Semi logarithmic *I*–*V* plots for (a) Au1/ZnO/In (b) Au2/ZnO/In, with varying temperature and in dark condition. (c) *I*–*V* plots of both Au contacts in dark at 80 and 300 K. (d) Energy band diagram at zero bias voltage.

Under the UV illumination, the photogenerated electrons tend to move towards the GZO while the photogenerated holes move towards the metal contacts. The interface states may be ionized by the accumulation of these hot carriers, modifying the local potential, which has been displayed by the band bending at interface of Fig. 3(d). In order to verify the assumed hypothesis, the Schottky barrier heights for two Au contacts is calculated using the equation $I = AA^*T^2 \exp(-q\Phi_b/K_BT)$ where I is the current through the Schottky barrier, A is the contact area, A^* is Richardson's coefficient, T is absolute temperature, and $q\Phi_b$ is the barrier height.[32] The values of $q\Phi_b$, as measured from the forward biased region in Fig. 3(c) at room temperature, show very little difference for Au1/GZO/In (0.342 eV) and Au2/GZO/In (0.345 eV). However, in the reverse bias region this difference is comparatively larger with 0.344 eV for Au1/GZO/In and 0.352 eV for Au2/GZO/In. Liu *et al.* have reported similar observations in ZnO film with electron concentration of order of 1×10^{17} cm^{-3}, due to trapping of carriers in the presence of trap states. In this case, GZO films having an electron concentration $\geq 10^{20}$ cm^{-3} the phenomenon is attributed to the ionization of interface states[33] on exposure to UV light. This ionization of interface states in highly conducting films enhances the free electron charge in conduction band and thereby shifting the quasi Fermi level to higher energies[34] resulting in lowering of barrier height and enhanced carrier tunnelling. There can be two-fold explanations behind higher zero bias photoresponse from our MSM-based UV PD as compared to others in literature, as shown in Table 2: (1) good crystalline quality of GZO film deposited by DIBSD system, (2) high electron concentration of the order of 10^{21} cm^{-3} and a very low electrical resistivity allow a significantly larger amount of photocurrent to pass between the electrodes under the exposure of UV illumination. The physical transport of electrons dominated by tunnelling under the effect of asymmetric Schottky barrier enables the device to operate at zero bias voltage.

Conclusions

In conclusion, highly conductive GZO film based UV photodetectors were fabricated by dual ion beam sputtering. Peak photoresponse of 58 mA W^{-1} at room temperature was observed at zero bias with a cut-off wavelength of 325 nm. The value of EQE at zero bias was ~22.5% and it reached to 48% at 1 V bias with an average photocurrent of 23 mA. A significantly higher value of IQE at zero bias was calculated to be 37.4%. The dissimilar characteristics of identically deposited electrodes due to process induced interface states were confirmed by temperature dependent *I–V* measurements. Tunneling of carrier across Au/GZO interface was observed due to high electron concentration and ionization of interface states.

Acknowledgements

The authors would like to acknowledge C. Mukherjee at RRCAT, Indore for technical support in deposition of Au electrodes, and Mukul Gupta at UGC-DAE Indore for performing SIMS measurement. Vivek Garg would like to thank UGC, New Delhi, for providing fellowship grant. This work is partially funded by DST and CSIR.

References

1 S. K. Pandey, V. Awasthi, S. Verma and S. Mukherjee, *Opt. Express*, 2014, **22**, 030983.
2 S. Verma, S. K. Pandey, M. Gupta and S. Mukherjee, *J. Mater. Sci.*, 2014, **49**, 6917.
3 D. Çalışkan, B. Bütün, M. C. Çakır, Ş. Özcan and E. Özbay, *Appl. Phys. Lett.*, 2014, **105**, 161108.
4 H. Shen, C. X. Shan, B. H. Li, B. Xuan and D. Z. Shen, *Appl. Phys. Lett.*, 2013, **103**, 232112.
5 K. W. Liu, B. Liu, S. J. Wang, Z. P. Wei, T. Wu, C. X. Cong, Z. X. Shen, X. W. Sun and H. D. Sun, *J. Appl. Phys.*, 2009, **106**, 083110.
6 L. J. Mandalapu, F. X. Xiu, Z. Yang and J. L. Liu, *Solid-State Electron.*, 2007, **51**, 1014.
7 L. C. Yang, R. X. Wang, S. J. Xu, Z. Xing, Y. M. Fan, X. S. Shi, K. Fu and B. S. Zhang, *J. Appl. Phys.*, 2013, **113**, 084501.
8 D. L. Jiang, L. Li, H. Y. Chen, H. Gao, Q. Qiao, Z. K. Xu and S. J. Jiao, *Appl. Phys. Lett.*, 2015, **106**, 171103.
9 J. Sun, F. J. Liu, H. Q. Huang, J. W. Zhao, Z. F. Hu, X. Q. Zhang and Y. S. Wang, *Appl. Surf. Sci.*, 2010, **257**, 921.
10 S. K. Pandey, S. K. Pandey, V. Awasthi, A. Kumar, U. P. Deshpande, M. Gupta and S. Mukherjee, *J. Appl. Phys.*, 2013, **114**, 163107.
11 S. Verma, M. K. Manna, S. K. Pandey, A. K. Das and S. Mukherjee, *RSC Adv.*, 2014, **4**, 62603.
12 J. C. Carrano, T. Li, P. A. Grudowski, C. J. Eiting, R. D. Dupuis and J. C. Campbell, *J. Appl. Phys.*, 1998, **83**, 6148.
13 Z. Bai, X. Yan, X. Chen, Y. Cui, P. Lin, Y. Shen and Y. Zhang, *RSC Adv.*, 2013, **3**, 17682.
14 P. N. Ni, C. X. Shan, S. P. Wang, X. Y. Liu and D. Z. Shen, *J. Mater. Chem. C*, 2013, **1**, 4445.
15 S. K. Pandey, S. K. Pandey, S. Verma, M. Gupta, V. Sathe and S. Mukherjee, *J. Mater. Sci.: Mater. Electron.*, 2013, **24**, 4513.
16 S. Liang and X. Bi, *J. Appl. Phys.*, 2008, **104**, 113533.
17 S. K. Pandey, S. K. Pandey, C. Mukherjee, P. Mishra, M. Gupta, S. R. Barman, S. W. D'Souza and S. Mukherjee, *J. Mater. Sci.: Mater. Electron.*, 2013, **24**, 2541.
18 P. K. Song, M. Watanabe, M. Kon, A. Mitsui and Y. Shigesato, *Thin Solid Films*, 2002, **411**, 82.
19 S. Kim, W. I. Lee, E.-H. Lee, S. K. Hwang and C. Lee, *J. Mater. Sci.*, 2007, **42**, 4845.
20 H. Y. Liu, V. Avrutin, N. Izyumskaya, Ü. Özgür, A. B. Yankovich, A. V. Kvit, P. M. Voyles and H. Morkoç, *J. Appl. Phys.*, 2012, **111**, 103713.
21 E. Fortunato, L. Raniero, L. Silva, A. Gonc-alves, A. Pimentel, P. Barquinha, H. Águas, L. Pereira, G. Gonc-alves, I. Ferreira, E. Elangovan and R. Martins, *Sol. Energy Mater. Sol. Cells*, 2008, **92**, 1605.
22 H. Y. Chen, K. W. Liu, X. Chen, Z. Z. Zhang, M. M. Fan, M. M. Jiang, X. H. Xie, H. F. Zhaoa and D. Z. Shen, *J. Mater. Chem. C*, 2014, **2**, 9689.
23 Z. Bai, X. Chen, X. Yan and X. Zheng, *Phys. Chem. Chem. Phys.*, 2014, **16**, 9525.

24 O. E. Semonin, J. M. Luther, S. Choi, H. Y. Chen, J. Gao, A. J. Nozik and M. C. Beard, *Science*, 2011, **334**, 1530.
25 W. B. Jackson, R. J. Nemanich, M. J. Thompson and B. Wacker, *Phys. Rev. B: Condens. Matter Mater. Phys.*, 1986, **33**, 10.
26 H. Fujiwara and M. Kondo, *Phys. Rev. B: Condens. Matter Mater. Phys.*, 2005, **71**, 075109.
27 T. Hashizume, J. Kotani and H. Hasegawa, *Appl. Phys. Lett.*, 2004, **84**, 4884.
28 G. Zhang, Y. Zheng and B. Wang, *J. Appl. Phys.*, 2013, **114**, 044111.
29 I. Hussain, M. Y. Soomro, N. Bano, O. Nur and M. Willander, *J. Appl. Phys.*, 2013, **113**, 234509.
30 H. L. Mosbacker, Y. M. Strzhemechny, B. D. White, P. E. Smith, D. C. Look, D. C. Reynolds, C. W. Litton and L. J. Brillson, *Appl. Phys. Lett.*, 2005, **87**, 012102.
31 L. J. Brillson, H. L. Mosbacker, M. J. Hetzer, Y. Strzhemechny, G. H. Jessen, D. C. Look, G. Cantwell, J. Zhang and J. J. Song, *Appl. Phys. Lett.*, 2007, **90**, 102116.
32 J. S. Liu, C. X. Shan, B. H. Li, Z. Z. Zhang, C. L. Yang, D. Z. Shen and X. W. Fan, *Appl. Phys. Lett.*, 2010, **97**, 251102.
33 S. N. Das, J. H. Choi, J. P. Kar, K. J. Moon, T. Lee and J. M. Myoung, *Appl. Phys. Lett.*, 2010, **96**, 092111.
34 G. Tabares, A. Hierro, J. M. Ulloa, A. Guzman, E. Muñoz, A. Nakamura, T. Hayashi and J. Temmyo, *Appl. Phys. Lett.*, 2010, **96**, 101112.